High-Density Integrated Optics

C. Manolatou, Steven G. Johnson, Shanhui Fan, Pierre R. Villeneuve, H. A. Haus,
and J. D. Joannopoulos

Abstract— This paper presents two-dimensional (2-D) finite difference time domain (FDTD) simulations of low-loss right-angle waveguide bends, T-junctions and crossings, based on high index-contrast waveguides. Such structures are essential for the dense integration of optical components. Excellent performance characteristics are obtained by designing the waveguide intersection regions as low-Q resonant cavities with certain symmetries and small radiation loss. A simple analysis, based on coupled mode theory in time, is used to explain the operation principles and agrees qualitatively with the numerical results.

Index Terms— Finite difference time domain (FDTD) methods, integrated optics, optical waveguide components, resonators, waveguide bends.

I. INTRODUCTION

THE strong light confinement in high index-contrast structures allows the design of waveguide components that can perform complex waveguide interconnections within a small area. High-performance right-angle bends and waveguide crossings that rely on resonances have been demonstrated in the context of photonic bandgap structures [1], [2]. In this work, we show that by modifying the waveguide intersection regions into resonant structures with symmetry, right angle bends, T-junctions and crossings with excellent transmission characteristics are also possible using conventional single-mode high index-contrast waveguides. These structures are viewed as two-, three-, and four-port resonant systems, respectively, connected to waveguides, and their behavior is explained using coupling of modes in time. Although valid only for weak coupling, such a model can still give an intuitive understanding of the operational principles. The basic idea relies on the fact that a lossless resonator with proper symmetry gives zero reflection and complete transmission on resonance. The presence of loss in the resonator causes reflection and lowers the transmission peak. This nonideal reponse can be improved by optimizing the coupling between the waveguide and the resonator modes.

These theoretical predictions are qualitatively verified by numerical simulations. In the literature, waveguide components are commonly simulated by the beam propagation method, which can only treat small angle bends and crossings and weakly guided structures. In this paper we use the finite difference time domain method (FDTD) which does not have such limitations. Because this method is computationally intensive, for ease of computation, we examine only two-dimensional (2-D) geometries. The computational domain is discretized into a uniform orthogonal mesh with cell size 20 nm and is terminated by Perfectly Matched Layer boundaries. The waveguides used in all the simulations have refractive index 3.2 surrounded by air and width 0.2 μm, chosen to ensure single mode operation over the entire bandwidth of the excitation. The fundamental mode of these waveguides is strongly guided with effective index 2.457 at 1.55 μm. The source is a 50-fs or 25-fs wide Gaussian pulse modulating a carrier at $\lambda = 1.55$ μm. The spatial dependence of the source is the fundamental waveguide mode profile which is calculated along a cross section of the 2-D waveguide (slab mode). The electric field polarization is chosen perpendicular to the plane. The power transmitted through a waveguide cross section is calculated for a range of frequencies as follows: The discrete Fourier transforms (DFT's) of all the field components along the cross section are calculated during the simulation as sums that are updated at each time step, and stored. The time stepping continues until all the fields in the computional domain have dropped to negligible values. At the end of the simulation the DFT's of the fields are used to calculate the component of the Poynting vector perpendicular to the cross section. By summimg the contributions of all the points, the transmitted power is obtained for the frequency range of interest.

The FDTD method was also used in [3] to simulate a collection of low-loss waveguide components for optical interconnects, similar to the ones presented here, that are based on multimoded low index-contrast structures and different operational principles.

For every waveguide component, we first show the field amplitude and the wavelength response of the unmodified junction, found numerically. Coupling of modes in time is used to qualitatively predict the behavior of the junction constructed as a cavity. Examples of the so modified junctions, their field distributions and wavelength responses found by FDTD are then presented.

C. Manolatou and H. A. Haus are with the Department of Electrical Engineering and Computer Science, Massachusetts Institute of Technology, Cambridge, MA 02139 USA.
S. G. Johnson, S. Fan, P. R. Villeneuve, and J. D. Joannopoulos are with the Department of Physics, Massachusetts Institute of Technology, Cambridge, MA 02139 USA.

II. 90° SHARP BENDS

Waveguide bends are basic structures for optical interconnects and therefore very important components in optical integrated circuits. Any abrupt directional change in dielectric
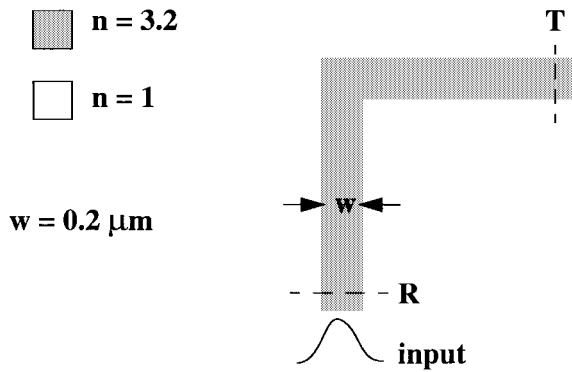
Fig. 1. Schematic of a 90° sharp waveguide bend made of a high index waveguide $n = 3.2$ surrounded by air. The cross sections where transmission and reflection are calculated are also shown.

waveguides causes a rotation of the phase fronts of the propagating modes. This perturbation causes mode conversion into unguided modes giving rise to radiation loss, mostly at the outer side of the corner. Proposed methods for reducing the radiation loss in waveguide bends include decelerating the phase-front inside the abrupt bend [4], accelerating the phase-front outside an abrupt bend [5], adding a microprism in the bend region [6] and replacing a bend with successive bends of smaller angle [7]. These studies were concerned with small-angle bends. For bends of larger angles corner reflectors have been proposed [8]. Low-loss 90°-bends with small radius of curvature and wide angle splitters made of high index-contrast waveguides (Si/SiO$_2$) have been reported in [9]. Their perfomance relies on strong confinement in these waveguides.

In this work, the performance of 90° sharp bends is greatly enhanced by placing a resonant cavity at the corner. A schematic of a simple 90° waveguide bend is shown in Fig. 1. The electric field in this bend and the transmission and reflection spectra are shown in Fig. 2(a) and (b), respectively. Due to mode mismatch at the corner a large fraction of the power is lost to radiation or reflected backward resulting in very poor transmission.

The waveguide bend is now modified by placing a resonant structure at the corner as shown in the schematic of Fig. 3. The idea is based on the principle of a symmetric resonator with two ports. At resonance, the transmission is complete with no reflection if the resonator is lossless. If this idea is applied to index guided structures, radiation loss is unavoidable leading to nonzero reflection and reduced transmission. The effects of radiation can be counteracted by making the external Q of the resonator very small. This is achieved by strong coupling of the waveguide modes to the resonator mode. This concept is simply explained using coupling of modes in time [10]. Because this analysis is based on perturbation theory, it can only provide a qualitative prediction in the case of strong coupling between the cavity and the waveguide modes. Following the approach of [10], the amplitude of the mode in the cavity is denoted by u and is normalized to the energy in the mode. The decay rates of the mode amplitude due to the coupling to the two waveguides are $1/\tau_{e1}$ and $1/\tau_{e2}$, respectively, related to the external Q's by $Q_{e1} = \omega_o \tau_{e1}/2$ and $Q_{e2} = \omega_o \tau_{e2}/2$, where ω_o is the resonance frequency.
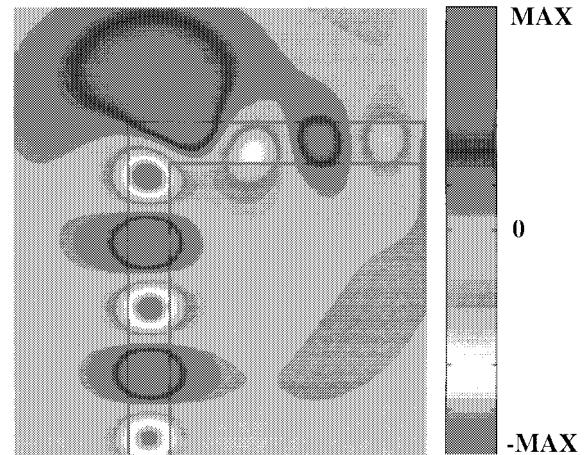
(a)
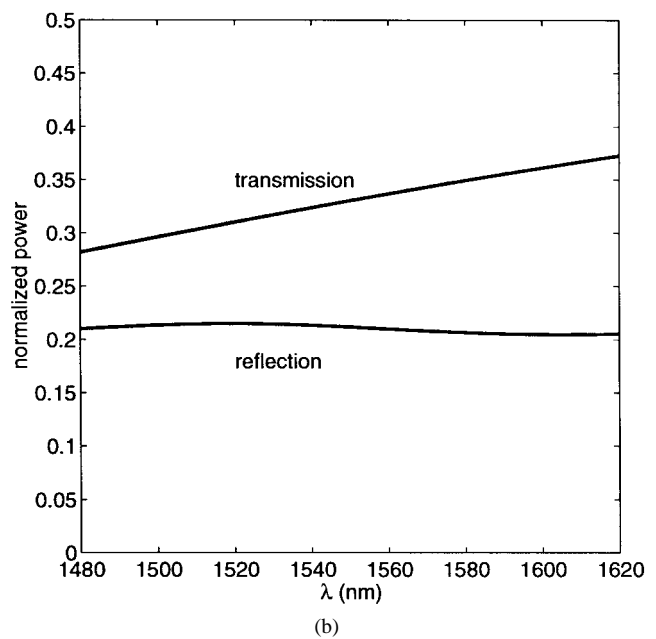
(b)

Fig. 2. (a) Electric field amplitude distribution in a plain 90°-bend. (b) Transmission and reflection spectra of the plain bend.
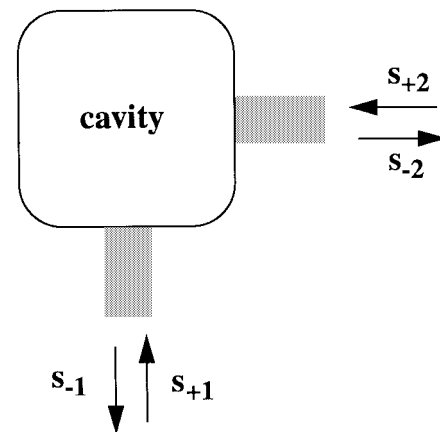

Fig. 3. Schematic of a two-port resonator connected to the waveguides of the 90°-bend.

The decay rate due to radiation loss is $1/\tau_o = \omega_o/2Q_o$. The incoming (outgoing) waves at the two ports are denoted by $s_{+1}(s_{-1})$ and $s_{+2}(s_{-2})$ (Fig. 3) and are normalized to the
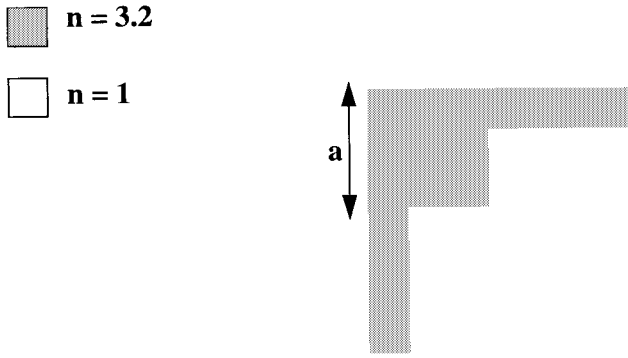
n = 3.2

n = 1

a

Fig. 4.   Corner region of bend modified by forming a square resonator inside the corner.

power carried by the waveguide mode. If the excitation is s_{+1} with a $e^{j\omega t}$ time dependence, and $s_{+2} = 0$ then at steady state we have [10]

$$u = \frac{\sqrt{\frac{2}{\tau_{e1}}} s_{+1}}{j(\omega - \omega_o) + \frac{1}{\tau_{e1}} + \frac{1}{\tau_{e2}} + \frac{1}{\tau_o}} \qquad (1)$$

and

$$s_{-1} = -s_{+1} + \sqrt{\frac{2}{\tau_{e1}}} u \quad s_{-2} = \sqrt{\frac{2}{\tau_{e2}}} u \qquad (2)$$

which, due to (1) finally give

$$\frac{s_{-1}}{s_{+1}} \equiv R = \frac{-j(\omega - \omega_o) + \frac{1}{\tau_{e1}} - \frac{1}{\tau_{e2}} - \frac{1}{\tau_o}}{j(\omega - \omega_o) + \frac{1}{\tau_{e1}} + \frac{1}{\tau_{e2}} + \frac{1}{\tau_o}} \qquad (3)$$

$$\frac{s_{-2}}{s_{+1}} \equiv T = \frac{\frac{2}{\sqrt{\tau_{e1}\tau_{e2}}}}{j(\omega - \omega_o) + \frac{1}{\tau_{e1}} + \frac{1}{\tau_{e2}} + \frac{1}{\tau_o}}. \qquad (4)$$

At $\omega = \omega_o$ the reflection is zero and the transmission maximized if

$$\frac{1}{\tau_{e1}} = \frac{1}{\tau_{e2}} + \frac{1}{\tau_o}. \qquad (5)$$

Thus, a symmetric system $(1/\tau_{e1} = 1/\tau_{e2} = 1/\tau_e = \omega_o/2Q_e)$ allows complete transmission at resonance provided that it is lossless. The width of the frequency response is determined by $1/\tau_e$. If loss is present the ratio $\tau_e/\tau_o = Q_e/Q_o$ determines the peak transmission and minimum reflection as

$$|R|^2 = \frac{\left(\frac{\tau_e}{2\tau_o}\right)^2}{\left(1 + \frac{\tau_e}{2\tau_o}\right)^2} \qquad |T|^2 = \frac{1}{\left(1 + \frac{\tau_e}{2\tau_o}\right)^2}. \qquad (6)$$

We modify the corner into a resonant cavity by increasing the volume of dielectric at this region to form a square resonator as shown in Fig. 4. Fig. 5(a) shows the electric field pattern of a bend with a square resonator of side $a = 0.62$ μm, defined in the schematic, where it can be seen that the radiation has been reduced compared with Fig. 2(a).
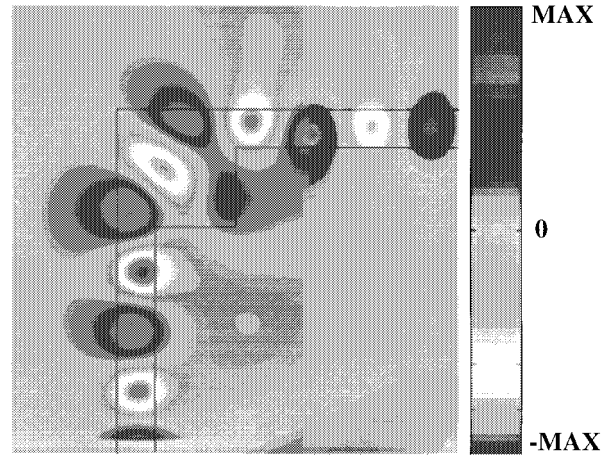
(a)
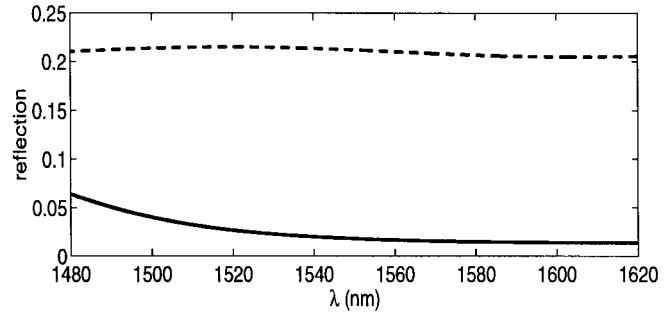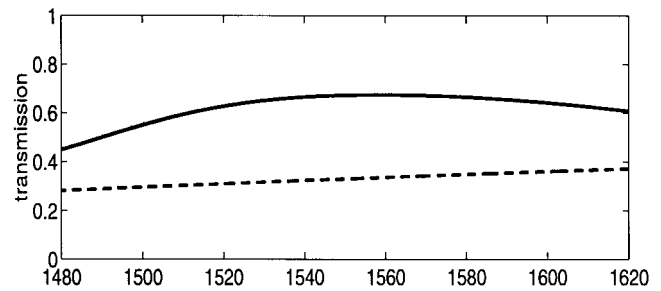
(b)

Fig. 5.   (a) Electric field amplitude in the modified bend for a square of side $a = 0.62$ μm. (b) Transmission and reflection spectra of the modified bend (solid line) compared with the plain bend (dashed line).

Comparing the spectra of the modified and unmodified bend in Fig. 5(b) we can see that the reflection has dropped by an order of magnitude and the peak transmission has more than doubled to about 70%. The performance is still poor because of considerable radiation loss that results in a relatively high ratio τ_e/τ_o in (6), estimated from the transmission peak to be 0.44. The Q_e and Q_o estimated from (4) are about 13 and 30, respectively.

In order to reduce the loss, we need a resonant cavity that is capable of steering the waveguide mode around the corner with very low radiation loss. This could be achieved by placing a quarter-disk at the corner as a curved Fabry–Perot resonator. The high index-contrast permits a very small radius of curvature without significant radiation loss. However, it is desirable to avoid curved interfaces that are harder to fabricate, so instead we further modify the corner by making a 45° cut
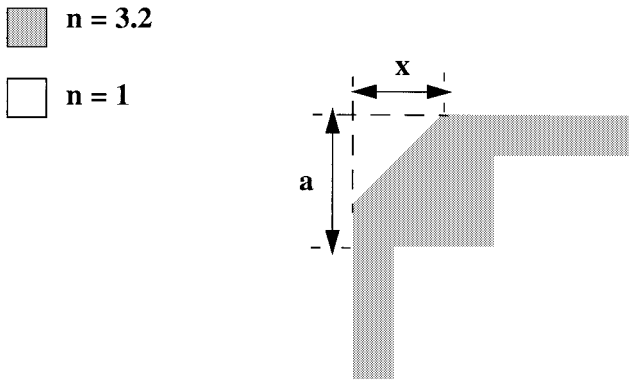
n = 3.2

n = 1

Fig. 6. Schematic of a square resonator at the bend with a 45°-cut at its outer corner.

(a)

(b)

Fig. 7. (a) Electric field amplitude in the modified bend, for $a = 0.72$ μm, and $x = 0.42$ μm. (b) Transmission and reflection spectra of the modified bend (solid line) compared to the plain bend (dashed line).

at the outer corner of the square as shown in the schematic (Fig. 6). In this configuration the strongly guided waveguide mode undergoes total internal reflection at the 45° cut and is guided around the modified corner by the outer walls.

The volume of dielectric in the structure determines the wavelength of maximum transmission and the depth x of the cut affects the bandwidth of the response. In the numerical simulations we have observed that as the depth of the cut is increased the transmission and the bandwidth increase up to a certain point. Further increase of the depth of the cut results in narrower bandwidth and slightly lower peak transmission. In order to keep the wavelength of maximum transmission around 1550 nm, the side of the square must be made larger to compensate for the dielectric taken out by the cut. In most of the cases we have examined, the best performance in terms of maximum transmission and bandwidth, is achieved when the depth of the 45° cut is such that the shape of the resonant structure of Fig. 6 is roughly a quarter of an octagon. In Fig. 7(a) and (b), we show the electric field amplitude and the spectrum for a quarter-octagon with $a = 0.72$ μm, $x = 0.42$ μm which resulted from the square of Fig. 4(b) by making a 45° cut and increasing the size to keep the center wavelength the same. The transmission is above 98% with a maximum of 98.6%, and the reflection is on the order of 10^{-4}, over a bandwidth of more than 120 nm. For comparison, we also show the field amplitude and spectrum of a quarter-disk of radius 0.68 μm in Fig. 8. The size of the quarter-disk was chosen to give a wavelength response as close as possible to that of the quarter-octagon. From the field patterns we see that the mode is guided mostly by the outer walls following almost the same path in both cases. An integer number of half wavelengths (in this case 3) "fit" in the modified corner as we would expect for a Fabry–Perot resonator.

In the above cases the strong coupling into the cavity leads to very low "loaded" Q and very wide transmission bandwidths, so the resonant nature is not obvious. In fact, the shape of the structure we have used combines the approaches of [4] and [8]. Resonant behavior can be seen more clearly if we make the cavity larger. Fig. 9(a) and (b) shows the field amplitude for cavities with $a = 1$ μm, $x = 0.58$ μm and $a = 1.2$ μm, $x = 0.70$ μm, respectively (roughly quarter octagons), that support higher order modes in the bandwidth
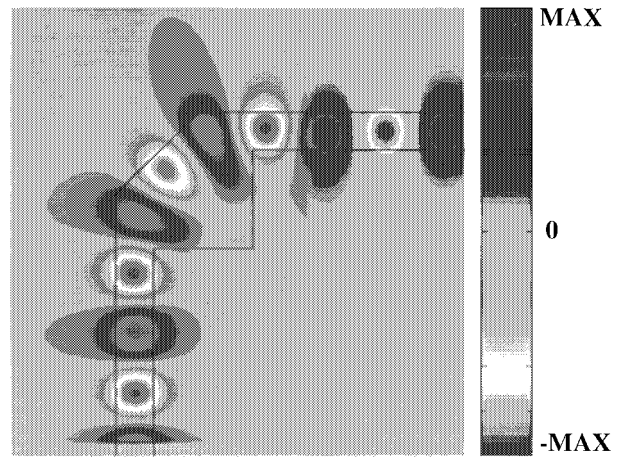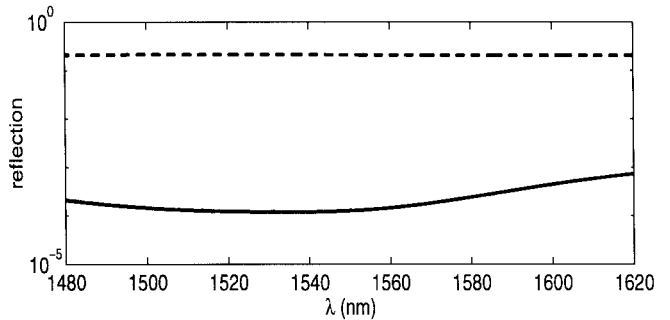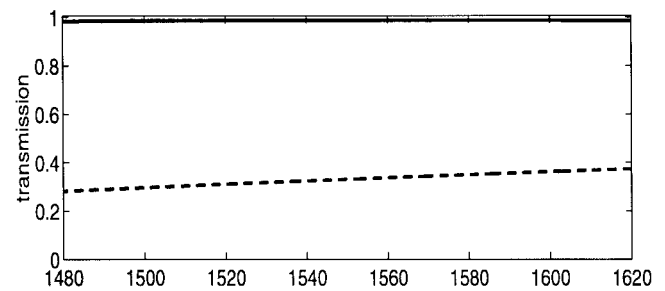
of interest. The electric field amplitude distributions show clearly that there is energy storage in the cavity, and that the mode pattern is not well matched to the waveguide mode. In Fig. 9(c) the transmission spectrum taken over a wider bandwidth shows that these structures support pairs of broad resonances closely spaced in wavelength that tend to merge into one very broad peak, as in the case of the larger cavity of Fig. 9(b). Similar behavior is suggested also by the shape and width of the transmission spectrum for $a = 0.72$ μm, shown in the same plot.

III. T-JUNCTION

A waveguide component useful for power splitting or combining is a T-junction which is essentially a Y-branch of 90° half-angle. Most studies in the literature have been concerned
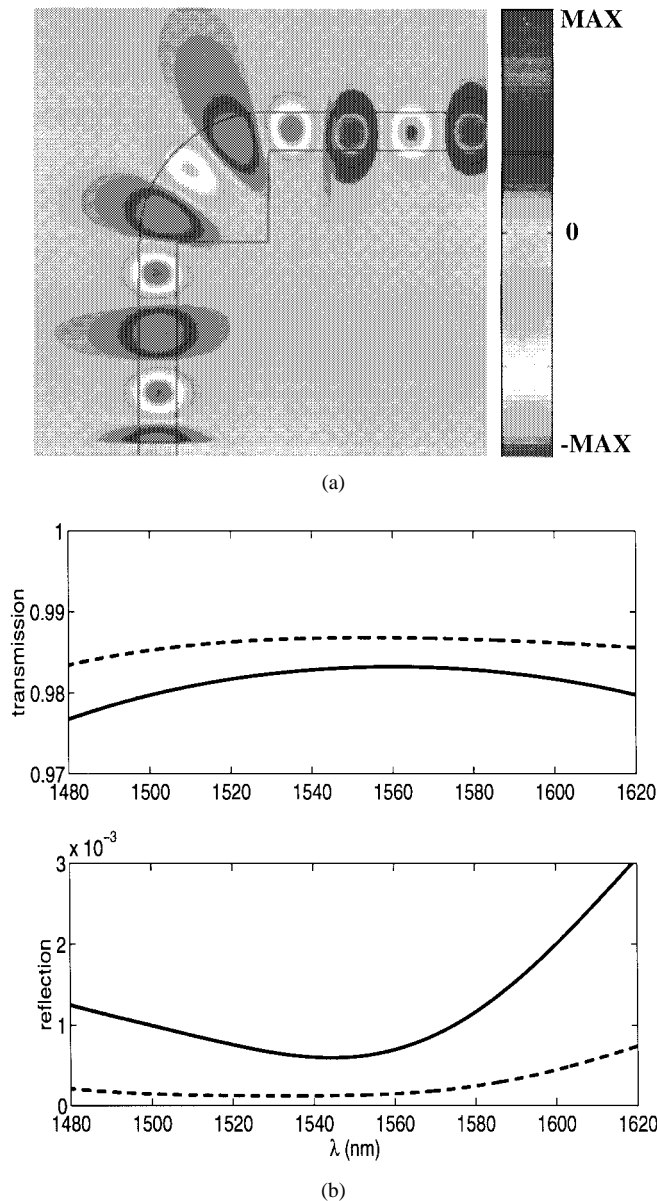
(a)

(b)

Fig. 8.   (a) Quarter-disk resonant cavity at the corner with radius 0.68 μm. (b) Comparison of the wavelength response for quarter-disk of radius 0.68 μm (solid line) and quarter-octagon of $a = 0.72$ μm (dashed line).

Fig. 9.   (a), (b) Electric field amplitude in larger cavities that reveals the energy storage (a) $a = 1$ μm, $x = 0.58$ μm (b) $a = 1.2$ μm, $x = 0.70$ μm. (c) Transmission and reflection spectra compared for $a = 0.72$ μm (solid line), 1 μm (dashed line) and 1.2 μm (dotted line).

Fig. 10.   Schematic of a plain T-junction made of a high index waveguide $n = 3.2$ surrounded by air. The cross sections where transmission and reflection are calculated are also shown.

with the design of small-angle Y-branches that require large device lengths to achieve a low-loss transition to the two arms. Index or height tapering have been used for adiabatic mode evolution [11], [12], and integrated microprisms have been proposed for phase-front compensation in a scheme analogous to that employed for loss reduction in bends [13].

The structures presented in the previous section for the low-loss bend can be used with small modifications in a T-junction. We consider first a plain T-junction shown in the schematic (Fig. 10). The electric field amplitude of a T-junction and the transmission and reflection spectra are shown in Fig. 11(a) and (b). Due to symmetry the transmitted power is equally distributed in the two outputs, therefore, the total power transmitted into the two ports is plotted to show the analogy with the 90°-bend.
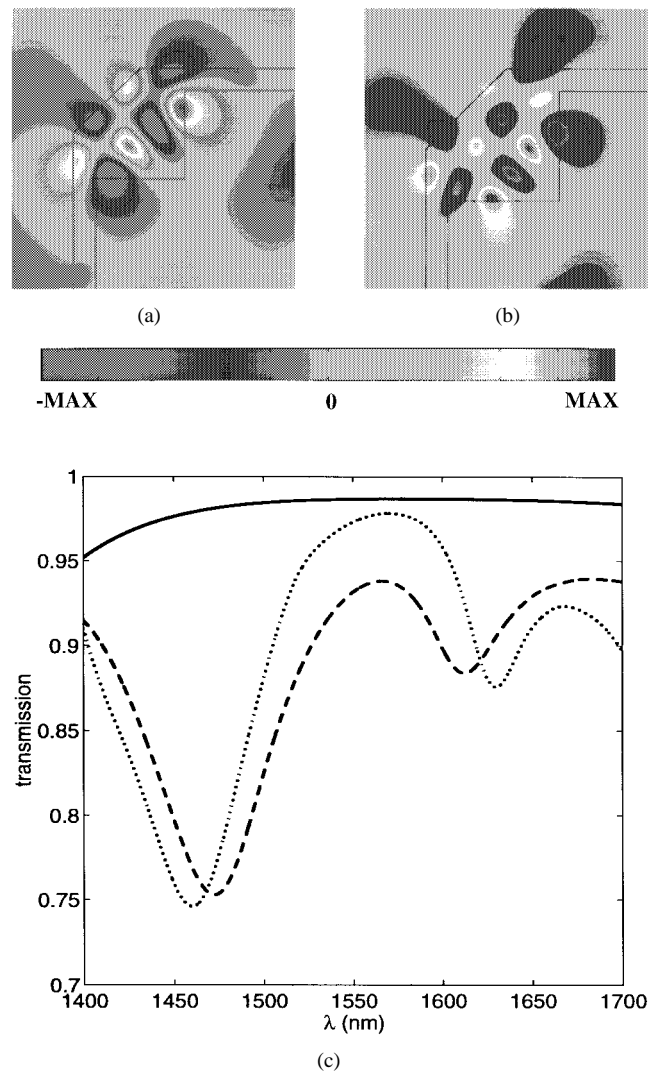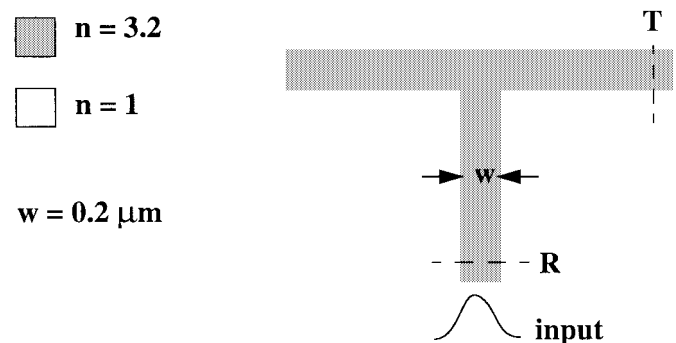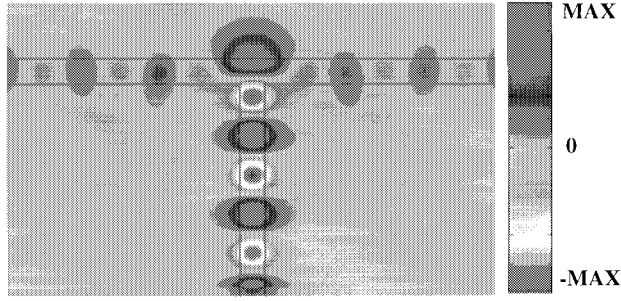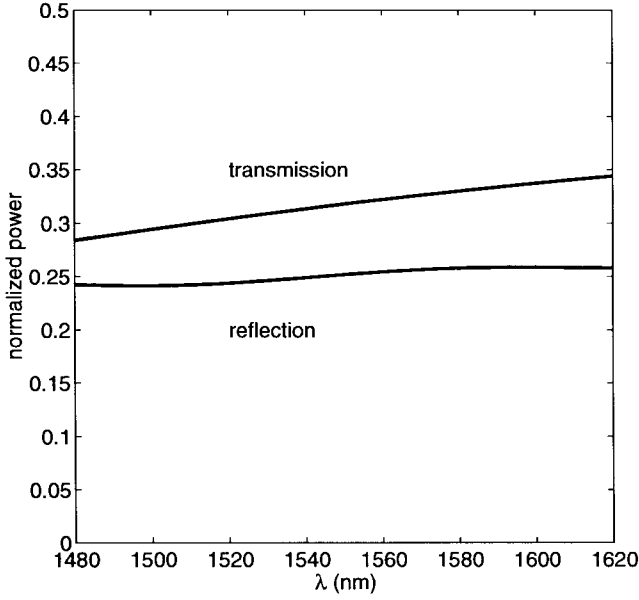
Placing a resonant cavity at the junction and treating the T-junction as a three-port system (Fig. 12), the analysis of Section II can be extended by defining incoming(outgoing) waves $s_{+3}(s_{-3})$ and adding a decay rate for the third port

(a)

(b)

Fig. 11. (a) Electric field amplitude in a plain T-junction. (b) Total transmission and reflection spectra of the plain T-junction.

$1/\tau_{e3}$. Exciting port 1 with s_{+1} at frequency ω we have

$$u = \frac{\sqrt{\dfrac{2}{\tau_{e1}}}}{j(\omega - \omega_o) + \dfrac{1}{\tau_{e1}} + \dfrac{1}{\tau_{e2}} + \dfrac{1}{\tau_{e3}} + \dfrac{1}{\tau_o}} s_{+1}. \quad (7)$$

The outgoing waves are given by expressions similar to (2) and due to (7) finally become

$$\frac{s_{-1}}{s_{+1}} \equiv R = \frac{-j(\omega - \omega_o) + \dfrac{1}{\tau_{e1}} - \dfrac{1}{\tau_{e2}} - \dfrac{1}{\tau_{e3}} - \dfrac{1}{\tau_o}}{j(\omega - \omega_o) + \dfrac{1}{\tau_{e1}} + \dfrac{1}{\tau_{e2}} + \dfrac{1}{\tau_{e3}} + \dfrac{1}{\tau_o}} \quad (8)$$

$$\frac{s_{-2}}{s_{+1}} \equiv T_L = \frac{\dfrac{2}{\sqrt{\tau_{e1}\tau_{e2}}}}{j(\omega - \omega_o) + \dfrac{1}{\tau_{e1}} + \dfrac{1}{\tau_{e2}} + \dfrac{1}{\tau_{e3}} + \dfrac{1}{\tau_o}} \quad (9)$$

$$\frac{s_{-3}}{s_{+1}} \equiv T_R = \frac{\dfrac{2}{\sqrt{\tau_{e1}\tau_{e3}}}}{j(\omega - \omega_o) + \dfrac{1}{\tau_{e1}} + \dfrac{1}{\tau_{e2}} + \dfrac{1}{\tau_{e3}} + \dfrac{1}{\tau_o}}. \quad (10)$$

From (8) we can see that in order to transfer the input power into ports 2 and 3 without reflection at resonance, the decay
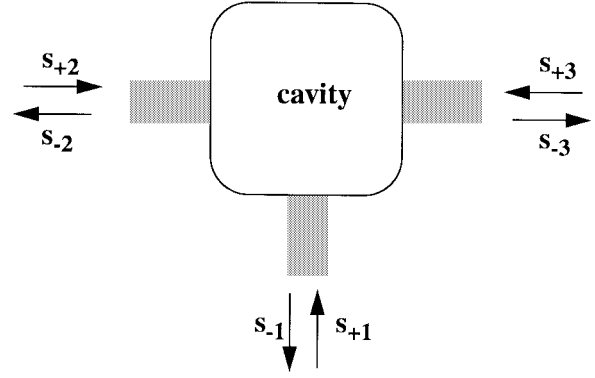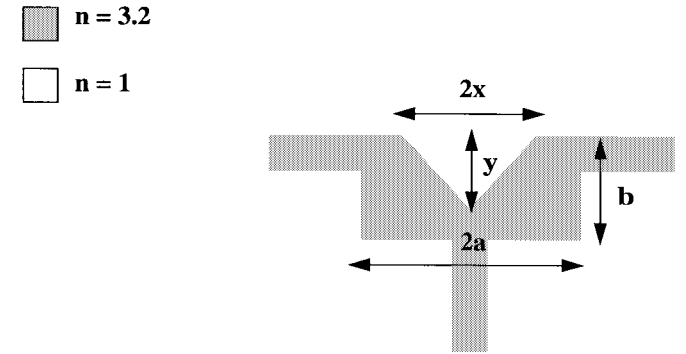

Fig. 12. Schematic of a three-port resonator connected to the waveguides of the T-junction.

Fig. 13. Modified T-junction for improved performance, resulting from two low-loss 90°-bends placed back-to-back.

rates must satisfy

$$\frac{1}{\tau_{e1}} = \frac{1}{\tau_{e2}} + \frac{1}{\tau_{e3}} + \frac{1}{\tau_o}. \quad (11)$$

The ratio of the power at the two output ports is then $|T_L/T_R|^2 = \tau_{e3}/\tau_{e2}$, so if $(1/\tau_{e2}) = (1/\tau_{e3})$ the power is equally split between the two ports. Note that for negligible loss, condition (11) is in agreement with the well known theorem of scattering matrix theory according to which it is impossible to match all three ports of a reciprocal lossless three-port system. Thus we cannot make a reflectionless Y-branch with three-fold symmetry $(1/\tau_{e1} = 1/\tau_{e2} = 1/\tau_{e3})$.

The choice of the resonant structure to be placed at the waveguide intersection follows from regarding the T-junction as two 90°-bends that look in opposite directions, placed back to back. As shown in Fig. 13, the modified T-junction employs a cavity that is made up of two strongly coupled cavities, each capable of directing a wave in one of the two directions as we have shown in Section II. The performance of the modified T-junction is improved by making the vertical side of the cavity shorter than the horizontal. Further improvement of the transmission and reflection response is obtained if the angle between the cut and the symmetry axis of the structure is made slightly smaller than 45°. The electric field amplitude for the best case, with $a = 0.72$ μm, $b = 0.66$ μm, $x = 0.40$ μm, $y = 0.44$ μm, is shown in Fig. 14(a) and the spectrum in Fig. 14(b). We can see that the behavior of this structure is remarkably similar to the low-loss 90°-bend. The maximum total transmission is close to 99% and the minimum reflection
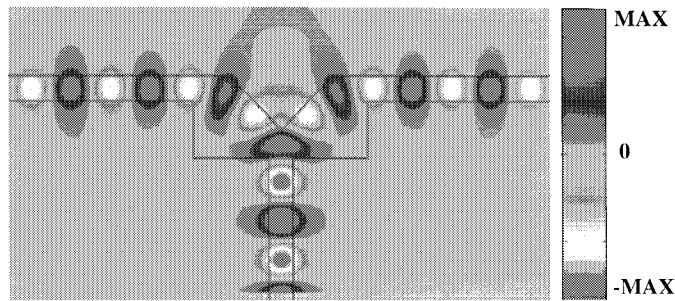
(a)
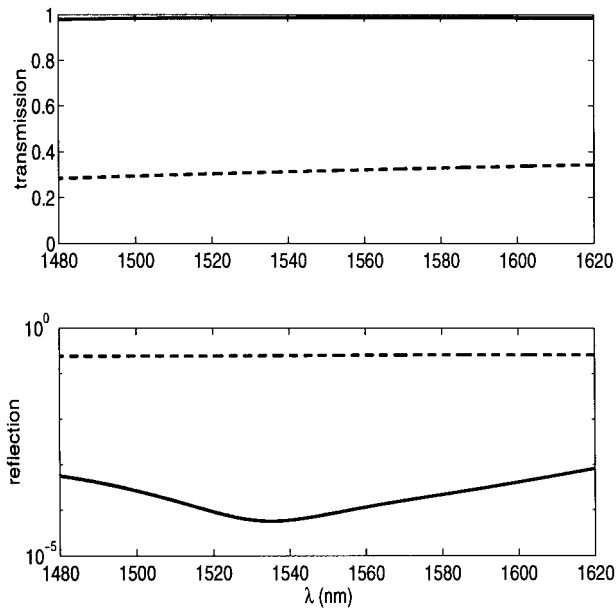
(b)

Fig. 14. (a) Electric field amplitude in a low-loss T-junction with $a = 0.72$ μm, $b = 0.66$ μm, $x = 0.40$ μm, $y = 0.42$ μm. (b) Transmission and reflection spectra of the modified T-junction (solid line) compared with the plain T (dashed line).

on the order of 10^{-4}. In analogy with the bend, larger resonant structures support higher order modes in the bandwidth of interest and the transmission curves show pairs of closely spaced broad resonances.

It is intreresting to see how the power distribution at the two ports changes, if the input waveguide is displaced from the symmetry plane of the cavity. Fig. 16 shows the transmission and reflection for different displacements d of the waveguide axis with respect to the symmetry plane of the cavity, defined in the schematic of Fig. 15. The symmetric T that we start from has $a = 0.70$ μm, $b = 0.66$ μm, and $x = y = 0.42$ μm. By moving the waveguide to the left, the transmission at the left port (port 2) increases. Although the total structure is no longer symmetric, the constraint (11) is still roughly satisfied as is suggested by the fact that the reflection remains low even for all the displacements from the center and the total transmitted power never falls below 95%. The field amplitude in the case that the waveguide wall coincides with the symmetry plane of the resonant structure ($d = 100$ nm) is shown in Fig. 17(a). The good performance of this asymmetric structure suggests that it is possible to make a low-loss branching structure by keeping the right part the
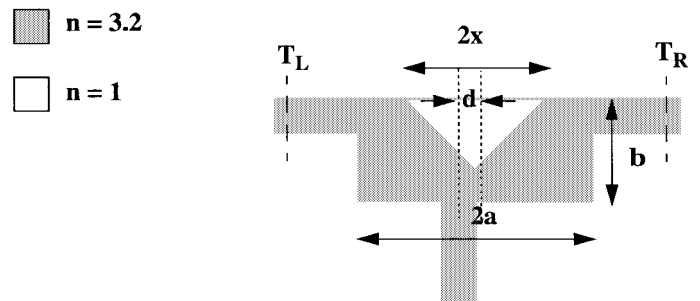

Fig. 15. Asymmetric T-junction resulting from displacing the input waveguide from the symmetry axis of the cavity.
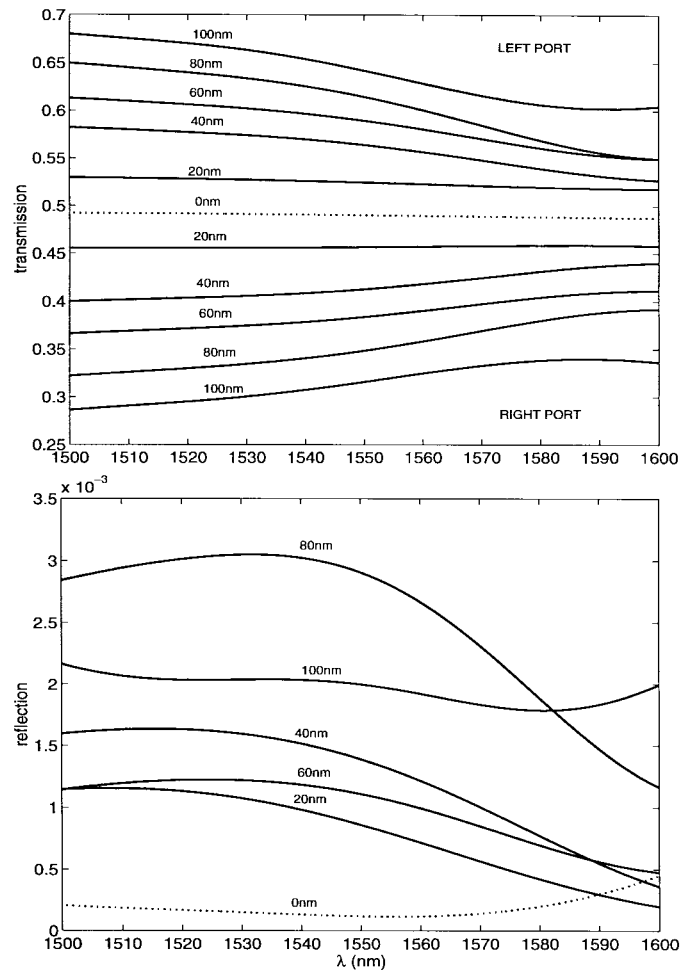

Fig. 16. Power distribution and reflection at the ports of an asymmetric T-junction for displacement of the input waveguide in the range from 0 to 100 nm.

same and replacing the left by a continuation of the input waveguide. The electric field amplitude for this case is shown in Fig. 17(b). The transmission and reflection spectra of the two asymmetric structures are very similar as we can see in Fig. 17(c). Therefore, proper choice of the cavity dimensions allows to tap off a certain percentage of the power from a straight waveguide with low loss and reflection.

IV. WAVEGUIDE CROSSINGS

Waveguide crossings are important components of an optical integrated circuit as they allow the interaction of many

(a)　　　　　(b)

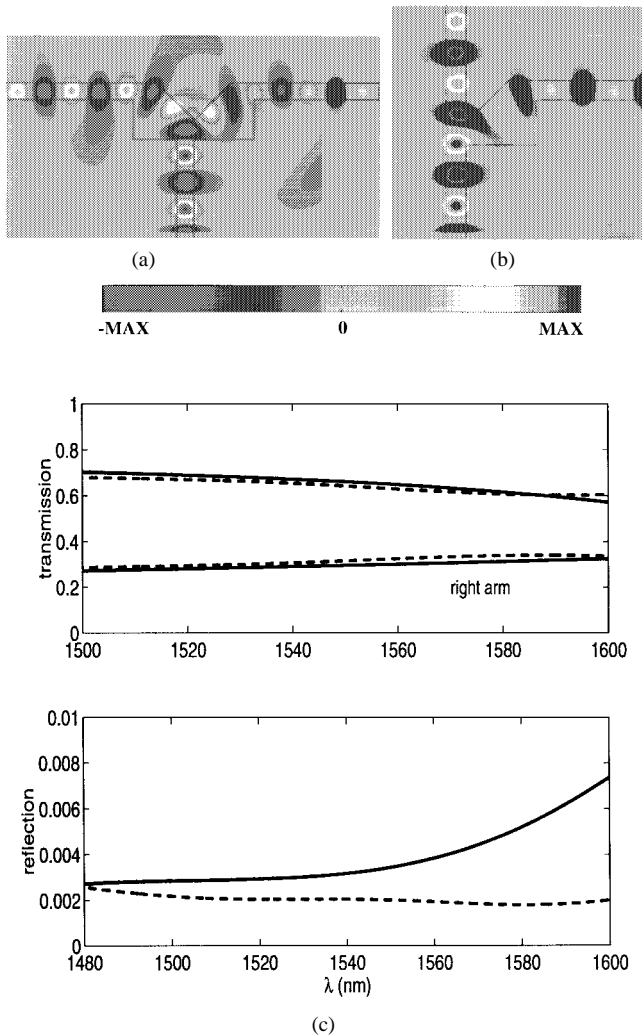-MAX　　　　　0　　　　　MAX

right arm

(c)

Fig. 17. Electric field amplitude in (a) asymmetric T with $d = 100$ nm and (b) branching structure resulting from asymmetric T. (c) Transmission and reflection spectra of branching structure (solid line) and asymmetric T (dashed line).

waveguides within a limited space. Ideally the wave launched in one of the intersecting waveguides must be fully transmitted forward without any power escaping sideways and with negligible reflection and radiation loss. Modification of the waveguide intersection for crosstalk reduction, has been employed elsewhere, e.g., [14], but for shallow angle crossings and with a penalty in throughput. The crosstalk at right angle crossings is very small when the waveguides are many wavelengths wide but close to 10% for waveguides on the order of the optical wavelengh as is the case in high index-contrast structures.

A high index-contrast waveguide crossing and the relevant cross sections for the calculation of transmission, crosstalk and reflection, are shown in Fig. 18. The electric field amplitude and the wavelength response are shown in Fig. 19(a) and (b), respectively. Although most of the input power is directed forward, nearly 10% of the input power escapes sideways leading to unwanted crosstalk. The way to achieve the desired performance is based again on the modification of the intersection into a resonant cavity. As explained in [2], the cavity

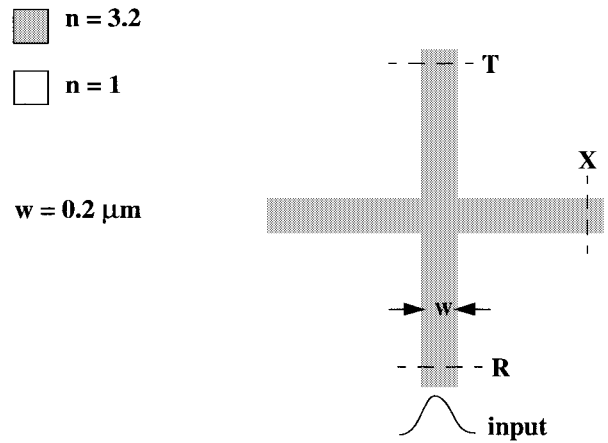$n = 3.2$

$n = 1$

$w = 0.2$ μm

Fig. 18. Schematic of a plain crossing of high index waveguides $n = 3.2$ in air, showing also the cross sections where transmission, crosstalk and reflection are calculated.
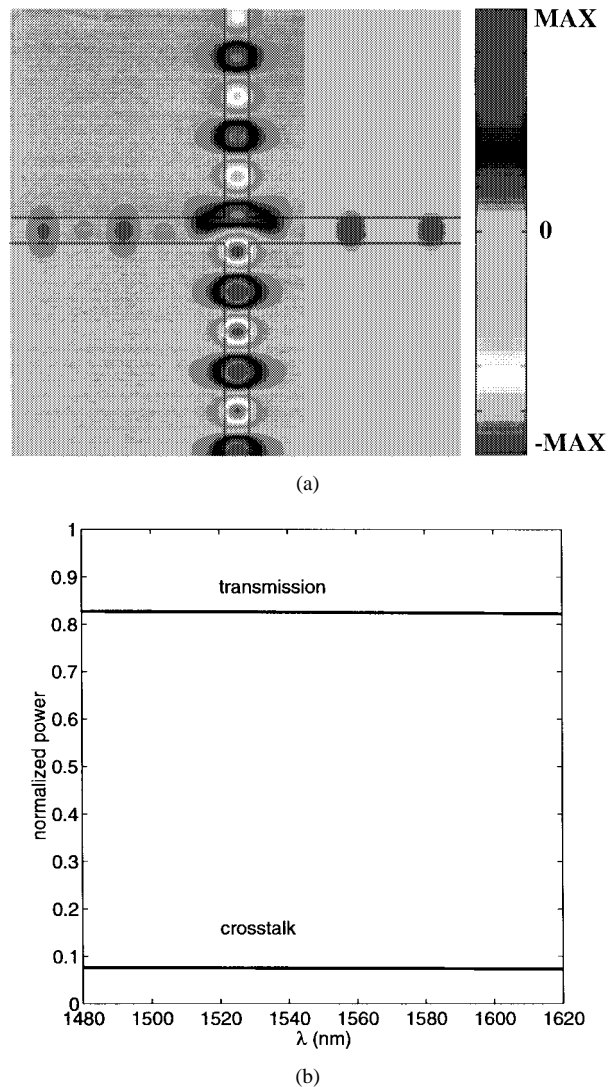

MAX

0

-MAX

(a)

transmission

crosstalk

(b)

Fig. 19. (a) Electric field amplitude in a plain waveguide crossing (b) Transmission and crosstalk spectra of the waveguide crossing.

must have fourforld symmetry and its symmetry planes must coincide with the waveguide axes. The cavity must support only two degenerate modes in the frequency range of interest,
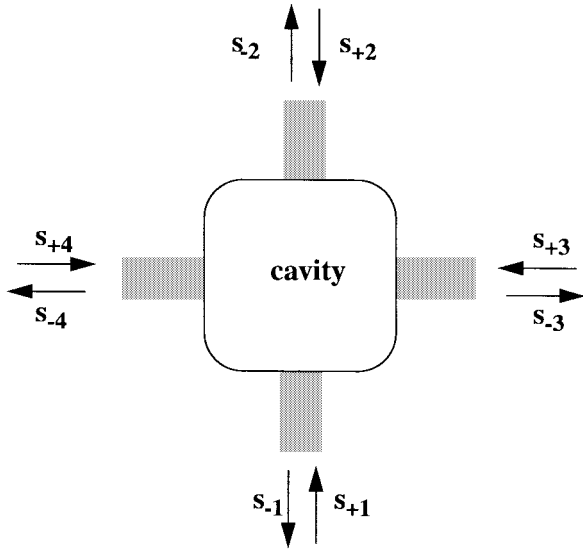
Fig. 20. Schematic of a four-port resonant cavity placed at the waveguide intersection.
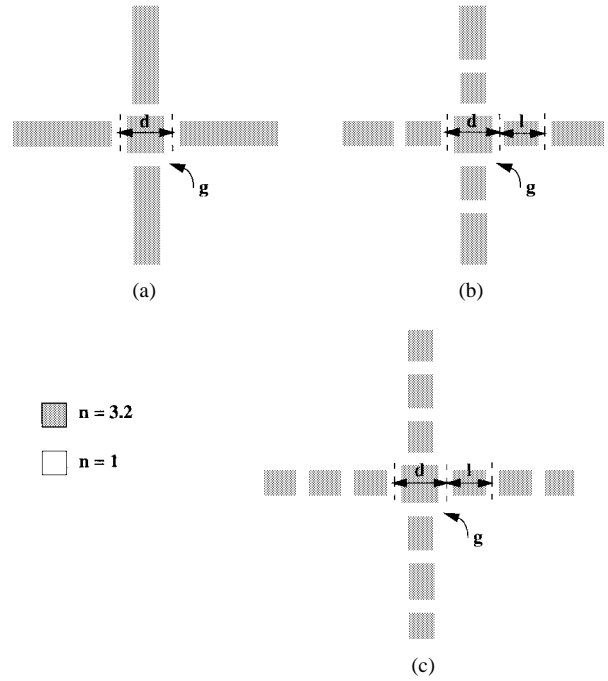

Fig. 21. Possible implementations of a cavity at the intersection with (a) one, (b) two, and (c) three, pairs of cuts on each of the crossing waveguides.

one mode with odd symmetry with respect to the horizontal waveguide axis and even symmetry with respect to the vertical waveguide axis, and one mode with the opposite symmetries. Under these conditions, each resonant mode will couple to the mode of just one waveguide and will be orthogonal to the mode of the perpendicular waveguide. Thus, excitation by the mode of the vertical waveguide will leave the other waveguide unexcited leading to full transmission with zero reflection (as discussed in Section II, for lossless cavity), and no crosstalk. This scheme has been tested in [2] by FDTD simulations in crosses made of photonic crystal waveguides and high index contrast waveguides with air holes, yielding up to eight orders of magnitude reduction in crosstalk.

We can use an alternative decomposition into symmetric modes to explain this idea with coupling of modes in time. The cavity at the intersection is regarded as a four-port system (Fig. 20), that supports two modes with the same resonant frequency ω_o. Due to the fourfold symmetry, each mode can be chosen to couple equally into all four ports. Their amplitudes are denoted by a and b and the decay rates into each port by $1/\tau_a$ and $1/\tau_b$, respectively. With input s_{+1}, at steady state we have

$$a = \frac{\sqrt{\dfrac{2}{\tau_a}}}{j(\omega - \omega_o) + \dfrac{4}{\tau_a}} s_{+1} \qquad b = \frac{\sqrt{\dfrac{2}{\tau_b}}}{j(\omega - \omega_o) + \dfrac{4}{\tau_b}} s_{+1}. \quad (12)$$

The desired behavior of the crossing is achieved if the two modes couple in phase into ports 1 and 2 and out of phase into ports 3 and 4. Then, assuming for simplicity real coupling coefficients and retaining only the relative phase between the two modes, the amplitudes of the outgoing waves are

$$s_{-1} = s_{+1} + \sqrt{\frac{2}{\tau_a}}a + \sqrt{\frac{2}{\tau_b}}b \qquad s_{-2} = \sqrt{\frac{2}{\tau_a}}a + \sqrt{\frac{2}{\tau_b}}b$$

$$s_{-3} = \sqrt{\frac{2}{\tau_a}}a - \sqrt{\frac{2}{\tau_b}}b \qquad s_{-4} = \sqrt{\frac{2}{\tau_a}}a - \sqrt{\frac{2}{\tau_b}}b \quad (13)$$

which, due to (12), give

$$\frac{s_{-1}}{s_{+1}} \equiv R = -1 + \frac{\dfrac{2}{\tau_a}}{j(\omega - \omega_o) + \dfrac{4}{\tau_a}} + \frac{\dfrac{2}{\tau_b}}{j(\omega - \omega_o) + \dfrac{4}{\tau_b}} \quad (14)$$

$$\frac{s_{-2}}{s_{+1}} \equiv T = \frac{\dfrac{2}{\tau_a}}{j(\omega - \omega_o) + \dfrac{4}{\tau_a}} + \frac{\dfrac{2}{\tau_b}}{j(\omega - \omega_o) + \dfrac{4}{\tau_b}} \quad (15)$$

$$\frac{s_{-3}}{s_{+1}} \equiv X_L = \frac{\dfrac{2}{\tau_a}}{j(\omega - \omega_o) + \dfrac{4}{\tau_a}} - \frac{\dfrac{2}{\tau_b}}{j(\omega - \omega_o) + \dfrac{4}{\tau_b}} \quad (16)$$

$$\frac{s_{-4}}{s_{+1}} \equiv X_R = \frac{\dfrac{2}{\tau_a}}{j(\omega - \omega_o) + \dfrac{4}{\tau_a}} - \frac{\dfrac{2}{\tau_b}}{j(\omega - \omega_o) + \dfrac{4}{\tau_b}}. \quad (17)$$

At ω_o the reflection and the transmission sideways are zero and the incoming signal is fully transmitted forward. If, in addition, $\tau_a = \tau_b = \tau_e = \omega/2Q_e$, the outputs at ports 3 and 4 remain zero at all frequencies. Then the frequency response at the ports 1 and 2 is essentially that of the symmetric two-port resonant system of Section II with decay rate $2/\tau_e$ at each port. Note that a and b are the sum and the difference, respectively, of the modes used in the analysis of [2].

Simple implementations of a cavity at the intersection are shown in Fig. 21. The numerical simulations reveal the dependence of the response on different design parameters. In the simple case (a), the resonance frequency is more strongly affected by the size of the block at the center. The width of the grooves determines the coupling into the cavity and
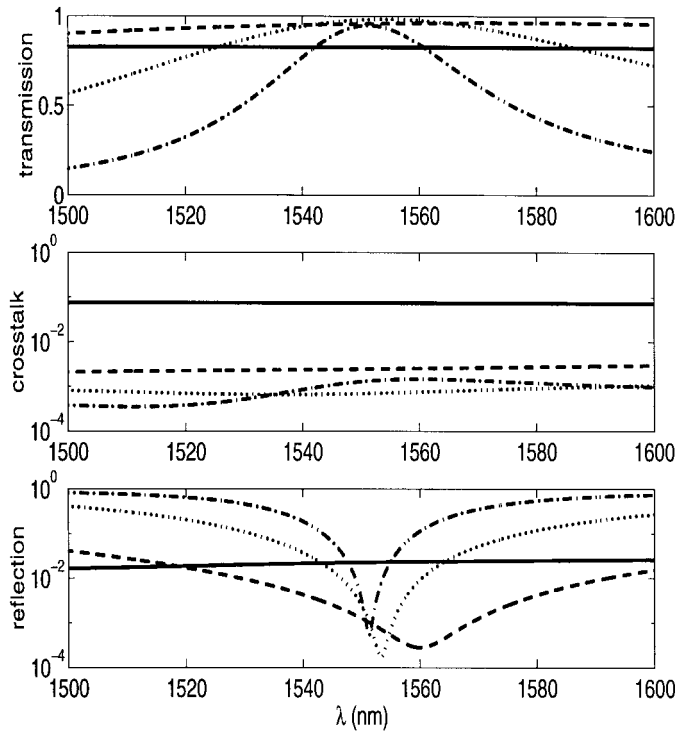
Fig. 22. Wavelength response for the three modified crossings compared with the plain crossing (solid line): one pair of cuts (dashed line), two pairs of cuts (dotted line), and three pairs cuts (dashed-dotted line).

in a smaller degree the resonance wavelength; wider grooves result in weaker coupling and therefore narrower resonance and the resonance shifts to shorter wavelength due to the lowering of the average dielectric. Similar effects occur by making more cuts. An additional pair of cuts as in case (b) yields narrower resonance, and further reduction of the crosstalk. The peak transmission is also increased because the radiation loss is greatly reduced in the cavity. Further increase of the number of cuts, as in (c), lowers the average dielectric and shifts the resonance to shorter wavelengths. Moreoover, assuming same radiation loss as in (b), the increase in the external Q due to weaker coupling leads to a slight decrease of the peak transmission. The best compromise for this particular configuration is when two cuts are made. The peak transmission for this case is 96% and the crosstalk less than 10^{-3}. The comparison of the spectra of all three cases with the plain cross is shown in Fig. 22 for $d = 0.44 \ \mu$m, $l = 0.36 \ \mu$m and $g = 80$ nm. The Q_e, associated with the coupling at each one of the four ports, and Q_o related to radiation losses, are estimated from (15) for $\tau_a = \tau_b$. We find approximately: (a) $Q_e = 10, Q_o = 130$, (b) $Q_e = 46, Q_o = 1000$, and (c) $Q_e = 130, Q_o = 1000$. The field patterns for cases (a) and (b) in Fig. 23, show a clear reduction of crosstalk with additional grooves.

V. DISCUSSION

We have shown that waveguide components for optical interconnections with excellent performance characteristics can be designed by placing a low-Q resonant cavity at the waveguide intersection, as predicted by coupling of modes in time

(a)

(b)

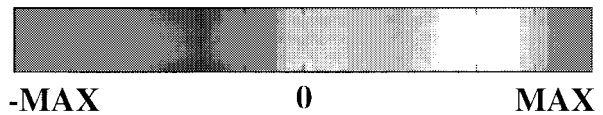-MAX   0   MAX
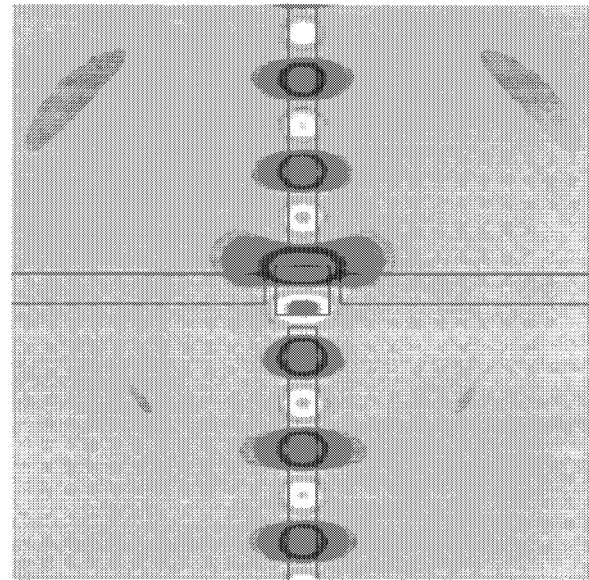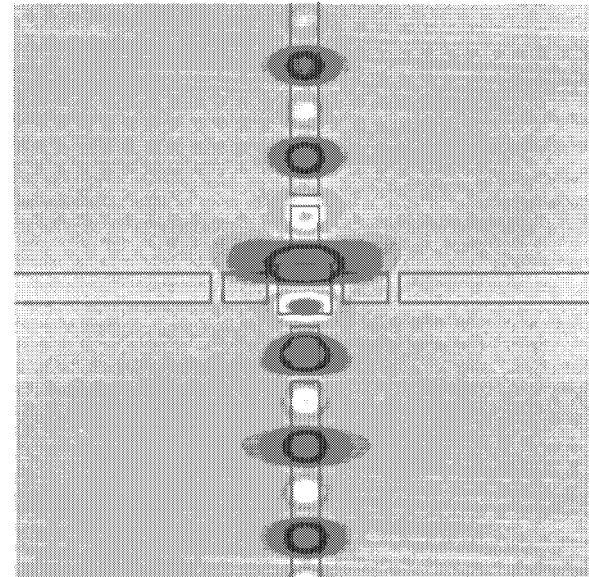
Fig. 23. Electric field amplitude for a cross with (a) one and (b) two pairs of cuts.

analysis. The success of this concept relies on the strong light confinement in high index-contrast waveguides, which allows the use of cavities on the order of the guided wavelength and with coupling to radiation much lower than the coupling to the waveguide. We have illustrated the operational principles by 2-D numerical simulations of a collection of example structures made of high index-contrast single-mode waveguides. The concept presented here is very general and could be applied using a variety of resonant structures, therefore our results do

not have the character of an optimized, finalized design. The numerical simulations showed that although the peak transmission is sensitive to small size changes, the wide bandwidth of the response allows a certain farbrication tolerance. Because we use open dielectric structures that employ index guiding, lowering the index contrast deteriorates the performance due to increased coupling to radiation. The size of the waveguides and resonators is strongly dependent on the material system and further investigation is required to reveal possible scaling laws. Another issue, characteristic of high index-contrast systems, is the polarization dependence which is expected to strongly affect the design and the performance. An accurate estimation of the polarization dependence as well as the leakage of radiation into the substrate requires 3D simulations for a more realistic design.

ACKNOWLEDGMENT

REFERENCES

[1] A. Mekis, J.C. Chen, I. Kurland, S. Fan, P. R. Villeneuve, and J. D. Joannopoulos, "High transmission through sharp bends in photonic crystal waveguides," *Phys. Rev. Lett.*, vol. 77, no. 18, pp. 3787–3790, 1996.

[2] S. G. Johnson, C. Manolatou, S. Fan, P. R. Villeneuve, J. D. Joannopoulos, and H. A. Haus, "Elimination of crosstalk in waveguide intersections," *Opt. Lett.*, vol. 23, no. 23, pp. 1855–1857, Dec. 1998.

[3] T. Doi, A. Iwata, and M. Hirose, "Analysis and design of low-loss and low mode-shift integrated optical waveguides using finite-difference time-domain method," *IEICE Trans. Electron.*, vol. E80-C, no. 5, pp. 625–630, 1997.

[4] E. G. Neumann, "Reducing radiation loss of tilts in dielectric optical waveguides," *Electron. Lett.*, vol. 17, no. 5 pp. 369–371, 1986.

[5] T. Shiina, K. Shirashi, and S. Kawakami, "Waveguide-bend configuration with low-loss characteristics," *Opt. Lett.*, vol. 11, no. 11, pp. 736–738, 1986.

[6] H. B. Lin, J. Y. Su, P. K. Wei, and W. S. Wang, "Design and application of very low-loss abrupt bends in optical waveguides," *IEEE J. Quantum Electron.*, vol. QE-30, pp. 2827–2835, Dec. 1994.

[7] H. F. Taylor, "Losses at corner bends in dielectric waveguides," *Appl. Opt.*, vol. 16, no. 3, pp. 711–716, 1977.

[8] K. Ogusu, "Transmission characteristics of optical waveguide corners," *Opt. Commun.*, vol. 55, no. 3, pp. 149–153, 1985.

[9] J. S. Foresi, D. R. Lim, L. Liao, A. M. Agarwal, and L. C. Kimerling, "Small radius bends and large angle splitters in SOI waveguides," *Proc. SPIE*, vol. 3007, p. 112–118, 1997.

[10] H. A. Haus, *Waves and Fields in Optoelectronics*. Englewood Cliffs, NJ: Prentice-Hall, 1984.

[11] M. H. Hu, J. Z. Huang, R. Scarmozzino, M. Levy, and R. M. Osgood Jr., "A low-loss and compact wavguide Y-branch using refractive index tapering," *IEEE Photon. Technol. Lett.*, vol. 9, pp. 203–205, Feb. 1997.

[12] ——, "Tunable Mach-Zehnder polarization splitter using height-tapered Y-branches," *IEEE Photon. Technol. Lett.*, vol. 9, pp. 773–775, June 1997.

[13] H. B. Lin, R. S. Cheng, and W. S. Wang, "Wide-angle low-loss single-mode symmetric Y-juntions," *IEEE Photon. Technol. Lett.*, vol. 6, July 1994.

[14] M. G. Daly, P. E. Jessop, and D. Yevick, "Crosstalk reduction in intersecting rib waveguides," *J. Lightwave Technol.*, vol. 14, pp. 1695–1698, July 1996.

C. Manolatou, photograph and biography not available at the time of publication.

Steven G. Johnson, photograph and biography not available at the time of publication.

Shanhui Fan, photograph and biography not available at the time of publication.

Pierre R. Villeneuve, photograph and biography not available at the time of publication.

H. A. Haus, photograph and biography not available at the time of publication.

J. D. Joannopoulos, photograph and biography not available at the time of publication.